



Σ^- PRODUCTION IN HIGH ENERGY PROTON INTERACTIONS

V. Hungerbuehler, R. Majka, J. N. Marx, P. Némethy
J. Sandweiss, W. Tanenbaum, and W. J. Willis
Yale University
New Haven, Connecticut 06520

and

M. Atac, S. Ecklund, P. J. Gollon, J. Lach, J. MacLachlan
A. Roberts, R. Stefanski, and D. Theriot
National Accelerator Laboratory
Batavia, Illinois 60510

and

C. L. Wang
Brookhaven National Laboratory
Upton, New York 11973

February 1973



Σ^- PRODUCTION IN HIGH ENERGY PROTON INTERACTIONS

V. Hungerbuehler, R. Majka, J. N. Marx, P. Némethy
J. Sandweiss, W. Tanenbaum, and W. J. Willis
Yale University, New Haven, Connecticut 06520*

and

M. Atac, S. Ecklund, P. J. Gollon, J. Lach, J. MacLachlan
A. Roberts, R. Stefanski, and D. Theriot
National Accelerator Laboratory, Batavia, Illinois 60510

and

C. L. Wang
Brookhaven National Laboratory, Upton, New York 11973†

ABSTRACT

Momentum spectra for forward Σ^- production on beryllium by protons of momentum 25.8 GeV/c and 29.4 GeV/c are presented. Data for the two primary proton momenta are compared for scaling behavior in the invariant cross section. In addition, the observed single particle momentum distributions are compared with single particle spectra from other inclusive reactions initiated by protons.

Using the Yale-NAL-BNL hyperon beam at the Brookhaven AGS, we have measured the momentum spectrum of Σ^- hyperons produced by 25.8 and 29.4 GeV/c protons on a beryllium target. We compare the Σ^- momentum distributions with the inclusive spectra of other particles produced in proton-initiated reactions and discuss these distributions in the light of the hypothesis of limiting fragmentation (HLF).¹

The experiment was performed during the spring of 1971 and summer of 1972. Figure 1 is a schematic representation of the hyperon beam and detection apparatus. A slow extracted beam of about 10^{11} protons per pulse interacts in a 0.26 in. \times 0.26 in. \times 10 in. Be target. The target is viewed at zero degrees and is followed by a curved, shielded magnetic channel 172 in. long. This length is sufficient to shield the downstream detectors from hadronic backgrounds produced in the target while limiting decay losses of Σ^- and Ξ^- hyperons to an acceptable level.

The inside walls of the second half of the channel are aluminized and tapered. When filled with freon gas, the channel acts as a threshold Cerenkov counter. Light beam particles (π^- , K^-) which form the most serious potential background are thus tagged and rejected.

The position and direction of the hyperons are measured by novel high resolution (100 μ m) spark chambers² placed immediately after the channel exit. These chambers operate with small gaps (1.2 mm) and high pressures (up to 15 atmospheres). They yield measurements of the hyperon momentum to $\pm 1\%$ and direction to ± 0.5 mrad with minimal decay loss in the spark chambers.

Downstream from the decay region are two magnet-spark chamber spectrometers, the first for analyzing the light decay products (mesons or electrons) and the second for analyzing the high-momentum decay proton from hyperon decay with a Λ^0 in the final state. These momenta are measured to an accuracy of better than 1%.

A hydrogen-filled threshold Cerenkov counter is used to select electrons for an experiment to study leptonic decays. A total-absorption scintillation-

counter calorimeter³ with the appropriate charged particle and gamma vetoes is located after the second spectrometer magnet. A pulse height requirement from the calorimeter allows the separation of muons from high-energy hadrons in the trigger. We thus use the calorimeter to identify fast neutrons and to give a crude measurement of their energy ($\pm 25\%$).

We report on data taken with the trigger (see Fig. 1): $\bar{C}_B \cdot B \cdot S \cdot NC \cdot \bar{V}_H \cdot \bar{V}_\pi$ where NC denotes a pulse height in the calorimeter greater than the muonic threshold level. This trigger selects events with a massive beam particle, a slow negative particle following the first spectrometer magnet, and a fast neutron following the second spectrometer magnet. This is the signature for the decay:

$$\Sigma^- \rightarrow n\pi^-.$$

The background in this trigger is less than 0.5%, consisting mainly of beam pions which are missed by the beam Cerenkov veto and charged particle vetoes. A scintillation counter telescope, looking at the hyperon production target, was used as a monitor of the interaction rate.

The data were taken in two series of runs, one for each primary proton energy. Within each series, individual runs were taken by varying the magnetic field in the shielded channel, thus changing the average hyperon momentum. Hyperon momenta from 17.0 to 26.6 GeV/c were studied in approximately 1 GeV/c steps. During the data runs at 25.8 GeV/c the rate of beam pion triggers ($C_B \cdot B \cdot S \cdot V_\pi \cdot \bar{V}_H$) was recorded to provide the normalization for the hyperon fluxes. For the 29.4 GeV/c runs the apparatus was triggered on beam pions at a rate prescaled to a convenient level. These events, which

consist of a single track in each of the spark chambers, as do the Σ^- events, were analyzed along with the Σ^- candidates. This procedure yields a Σ^-/π^- production ratio which is independent of spark-chamber performance.

After cuts were applied to eliminate decays occurring upstream from the defined decay region and to define the fiducial volume, events were reconstructed under the hypothesis of the decay $\Sigma^- \rightarrow n\pi^-$. This once over-constrained reaction is used to calculate the mass of the decaying hyperon. A typical mass spectrum is shown in Fig. 2. This spectrum is well reproduced by a Monte-Carlo program when experimental resolution is included.

The ratio Σ^-/π^- produced at the target is shown in Fig. 3 with numerical values given in Table I. The data have been corrected for acceptance of the magnetic channel, efficiency of the detection apparatus, and lifetime loss. An empirical fit⁴ to π^- production on Be was then used to calculate the Σ^- momentum spectrum from the Σ^-/π^- ratio. The resulting Σ^- production spectra are presented in Table I.

Figure 4 shows the invariant cross section for Σ^- production

$$\frac{E d^3 \sigma}{d^3 p} = \frac{E}{2} \frac{d^3 \sigma}{dp d\Omega}$$

plotted as a function of α . Here p and E are the momentum and total energy of the produced particle and α is its laboratory momentum normalized to its kinematic limit. Within the accuracy of these measurements we feel that our two sets of data are consistent with the invariant cross-section scaling in the variable α . Future measurements of Σ^- productions at higher energies will provide further tests of this scaling behavior.⁵

In Fig. 4 we also plot the observed invariant cross sections for several inclusive processes $p + \text{Be} \rightarrow C + X$. Again the data are plotted with outgoing momenta of the observed outgoing particle, C , normalized to the kinematic limit. The Σ^- data is from this experiment and the other curves are derived from the data of Allaby et al.⁶

The errors indicated in all graphs and tables in this paper are statistical only. However, there are several sources of possible systematic normalization errors. Uncertainties in the spark-chamber efficiency for the 25.8 GeV/c data, the Σ^- lifetime, and the Monte-Carlo calculation of the channel and detection apparatus acceptance contribute an additional systematic uncertainty of about 10%.

We have compared these results with the recent experiment⁷ performed at CERN measuring Σ^- production at 10 mrad at a primary proton beam momentum of 24.0 GeV/c. At a given value of α the Σ^- yields per interacting nucleon agree to within 20%. The Σ^-/π^- ratios of Ref. 7 are higher by about a factor of two but these results are consistent if the difference in production angles is taken into account.

Our data may be viewed in the context of the HLF as put forth by Yang and co-workers.¹ Single particle inclusive spectra are thought to approach their kinematic limits differently if the observed particle is favored or disfavored, i. e., depending on whether quantum numbers are changed. For $p + \text{Be} \rightarrow C + X$, $C = \text{proton}$ is favored while $C = \pi^+, \pi^-, K^+, K^-, \bar{p}, \Sigma^-$ are disfavored. The predicted behavior is quite evident from these data. However, we note that the Σ^- spectrum of Fig. 4 displays attributes of both

avored and disfavored spectra. For $\alpha < 0.9$ it is relatively flat, like the proton spectrum, while near the kinematic limit the behavior is like other disfavored distributions. The simple picture of quantum number exchange determining the general features of inclusive distributions must be modified to account for the nature of the quanta exchanged.

We wish to thank our engineering staff, Satish Dhawan, Cordon Kerns, Blaise Lombardi, and Irving Winters and our technicians Jon Blomquist, Ed Steigmeyer, and Alan Wandersee for their help in the design and setup of the apparatus. We thank the University of Michigan group for the use of their scintillation counter calorimeter. We also thank the AGS staff, in particular David Berley for providing the technical support needed for the success of this experiment.

REFERENCES

* Research supported by the U. S. Atomic Energy Commission under contract AT(11-1) 3075.

† Work supported by the U. S. Atomic Energy Commission.

¹ J. Beneke et al., Phys. Rev. 188, 2159 (1969).

² W. J. Willis et al., Nucl. Instr. and Methods 91, 33 (1971).

³ M. Atac et al., Nucl. Instr. and Methods 106, 389 (1973).

⁴ C. L. Wang, Phys. Rev. Letters 25, 1068 (1970).

⁵ Yale-NAL Collaboration, NAL Proposal 97 (unpublished).

⁶J. V. Allaby et al. , CERN Report 70-12 (1970).

⁷J. Badier et al. , Phys. Letters 39B, 414 (1972).

⁸T. T. Chou and C. N. Yang, Phys. Rev. Letters 25, 1072 (1970).

Table I. Σ^-/π^- Production Ratios and Forward Σ^- Production Laboratory Cross Sections for Protons on Beryllium.

A. 25.8 GeV/c Incident Protons		
Secondary Momentum GeV/c	Σ^-/π^-	$d^3\sigma/dp d\Omega$ mb (sr GeV/c) ⁻¹
17.75	0.329±0.042	14.41±1.8
18.75	0.465±0.048	13.3 ±1.4
19.75	0.669±0.067	12.0 ±1.2
20.75	1.08 ±0.077	11.7 ±0.8
21.75	2.41 ±0.14	14.9 ±0.9
22.75	2.85 ±0.14	9.4 ±0.5
23.75	21.91 ±1.4	4.0 ±0.2
B. 29.4 GeV/c Incident Protons		
Secondary Momentum GeV/c	Σ^-/π^-	$d^3\sigma/dp d\Omega$ mb (sr GeV/c) ⁻¹
17.0	0.185±0.011	25.3±1.5
19.0	0.263±0.016	19.0±1.2
20.0	0.374±0.022	19.0±1.1
20.5	0.380±0.021	16.3±1.0
21.0	0.463±0.028	16.3±1.0
22.0	0.648±0.037	15.3±0.9
23.45	1.19 ±0.07	15.0±0.9
25.0	1.72 ±0.16	10.1±0.9
26.0	2.62 ±0.16	6.0±0.4

HIGH ENERGY NEGATIVE HYPERON BEAM

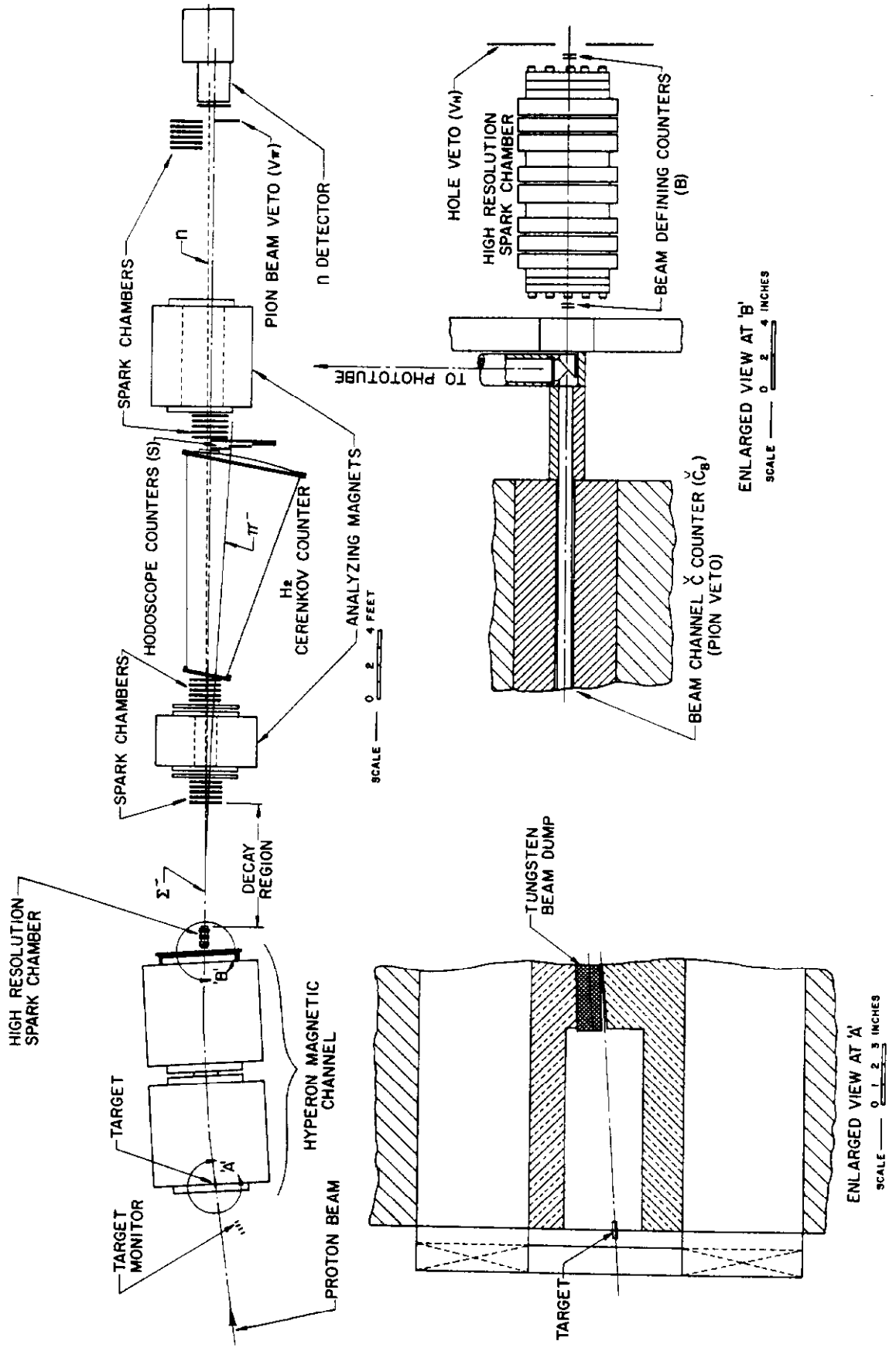


Fig. 1. Schematic diagram of the high-energy hyperon beam at the BNL, AGS.

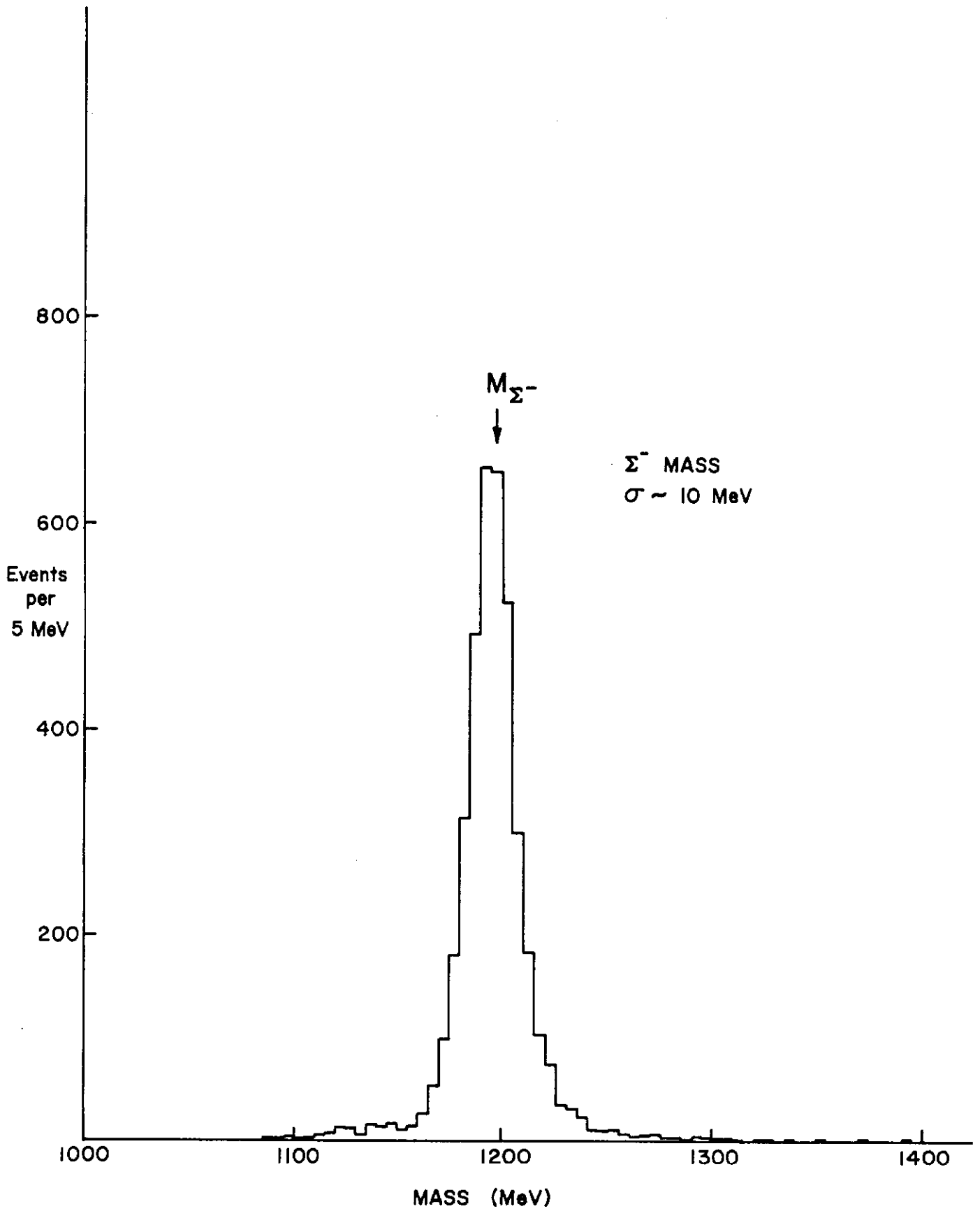


Fig. 2. Typical Σ^- reconstructed mass spectrum.

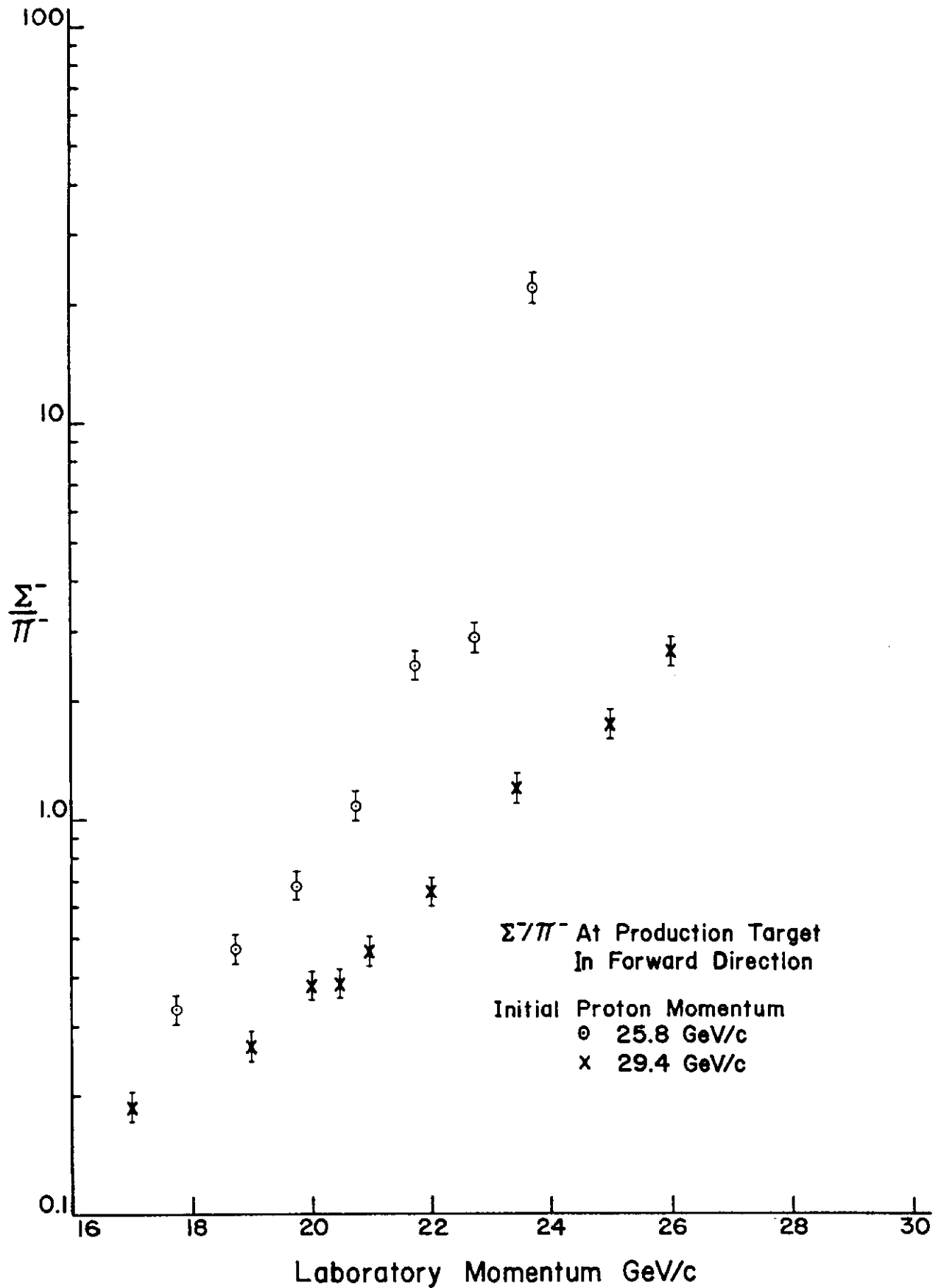


Fig. 3. Σ^-/π^- production ratios in the forward direction for 28.5 and 29.4 GeV/c protons on Be.

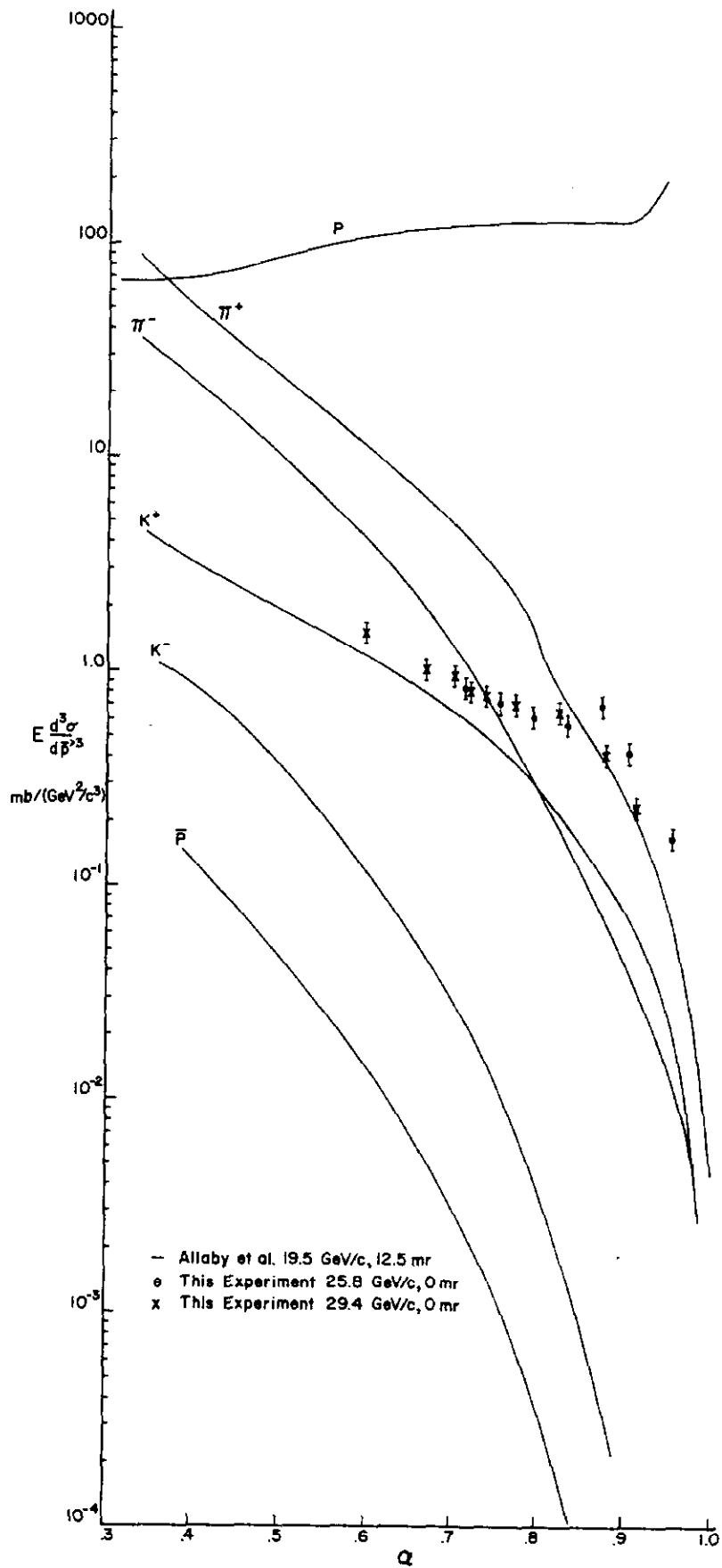


Fig. 4. The invariant inclusive cross section plotted as a function of the longitudinal laboratory momentum normalized to its kinematic limit for various particles produced in proton Be collisions.